Rotation of Structural Water inside a Protein: Calculation of the Rate and Vibrational Entropy of Activation

Stefan Fischer*,†

Computational and Structural Chemistry, Hoffmann-La Roche/Pharma Research, C H-4070 Basel, Switzerland

Chandra S. Verma*,‡ and Roderick E. Hubbard

Protein Structure Group, Department of Chemistry, University of York, U.K.

Received: September 10, 1997; In Final Form: December 10, 1997

Water molecules buried inside a protein are often considered as an integral part of the structure and are increasingly used as NMR probes to study the dynamics of proteins (Denisov, V.; Peters, J.; Horlein, H. D.; Halle, B. *Nat. Struct. Biol.* **1996**, *3*, 505). The present calculations give new insights into the mobility of such structural water. Reaction path calculations using conjugate peak refinement (Fischer, S.; Karplus, M. *Chem. Phys. Lett.* **1992**, *194*, 252) are carried out to compute the transition state and activation energy (9.7 kcal mol^{-1}) for the rotation of a water molecule buried in the protein bovine pancreatic trypsin inhibitor. These are compared to the values calculated (10−12.3 kcal mol^{-1}) for the same process in ice, for which the experimental value has been determined (12.8 ± 0.9 kcal mol^{-1}). The process, which results in the interchange of the two water hydrogens, is similar in both systems. It is not a simple C2-flip of the buried water, but a complex motion involving two successive rotations around orthogonal axes. A normal-mode analysis performed on the ground and transition states of the protein enables the correction for the vibrational entropy to be included in the derivation of the rotational correlation time (45 ns) of the buried water. Vibrational frequencies up to 620 cm^{-1} are found to contribute, thus requiring the inclusion of quantum effects. A fluctuation frequency of 20−50 cm^{-1} along the curvilinear reaction path is derived, which leads to a vibrational entropy of activation of 8.6 cal mol^{-1} K^{-1}.

Introduction

The importance of structural solvent in proteins is well-recognized,[1,2] but little is known about the behavior of this buried solvent.[3] While some progress has been made toward a better understanding of the role of water in proteins,[4−10] experimental data about the dynamics of water molecules buried in a protein has only recently been available.[1,2,6,9,11−13] Denisov et al.[13] have measured the rate of exchange with bulk water of a structural water molecule in the protein bovine pancreatic trypsin inhibitor (BPTI) by nuclear magnetic relaxation dispersion (NMRD).[11,13−16] The underlying assumption in such measurements is that any rotation of this buried water molecule is significantly slower than the tumbling of the protein,[13−16] whose rotational correlation time was determined to be 9.7 ns at 300 K for BPTI.[13] We examine this hypothesis by analyzing the rotational isomerization of this buried water molecule, numbered W122,[17] with the help of the conjugate peak refinement (CPR) method.[18] This method is well-suited for the study of activated processes that occur on a time scale that is longer than can be simulated by standard molecular dynamics. It gives a time-independent description of the reaction in terms of the essential motions along the minimum-energy path, the transition state structure(s), and the corresponding energy barrier(s). For comparison, we also calculate the rotation path of a water molecule in ice Ih,[19] for which the reaction rate has been measured experimentally.[20] We find that the only allowed rotation for a buried water molecule is a flip leading to the interchange of its two hydrogen atoms. This process, which is similar in both systems, is not a simple rotation around the C2-symmetry axis of the water molecule, but a succession of two rotations around orthogonal axes. This complex motion accounts for a lower than expected potential energy barrier for W122/BPTI (9.7 kcal mol^{-1}). In ice, the calculated barrier is 12.3 kcal mol^{-1}, close to the experimental Arrhenius activation energy of 12.8 ± 0.9 kcal mol^{-1}.[20] A normal-mode analysis[21] performed both in the ground state and at the transition state of W122/BPTI enables the derivation of a vibrational entropy of activation (8.6 cal mol^{-1} K^{-1}) for the first time in a system as large as a protein. Vibrational frequencies as high as 620 cm^{-1} are found to contribute to the entropy, and hence quantum effects have to be included. We determine a pertinent fluctuation frequency for the motion along a curvilinear reaction path, which is a libration of water W122 at a frequency of 20−50 cm^{-1}. On the basis of this data, we find that the correlation time of water rotation inside the protein is on the order of 45 ns, much faster than previously assumed.

Methods and Theory

Reactant and Product Structures. The crystal structures of ice-Ih[19] and BPTI (PDB entry 5pti;[17] resolved at 1.0 Å) were used for this study. The ice model consisted of 288 nonperiodic water molecules corresponding to 72 unit cells of the ice crystal (space group *P*63/*mmc*). The 63 structural water molecules of the crystal were included in the BPTI model (5 additional water molecules were placed into the phosphate and the potassium binding sites). We employed the empirical energy function of the program CHARMM[22] with the TIP3P model for water[23] and the parameter set 19 for the protein,[24] but using explicit hydrogen atoms on all aromatic groups (from parameter set 22[25]) to account for their non-negligible quadrupole moment. The

† E-mail: stefan.fischer.sf2@roche.com.
‡ E-mail: chandra@yorvic.york.ac.uk.

S1089-5647(97)02948-9 CCC: $15.00
Published on Web 02/18/1998

fact that a proton can be shared in ice by two neighboring oxygen atoms[19,20,26] was neglected in these calculations. The structures were prepared by minimization under decremental constraints as described previously.[27,28] The final minimized structures, in which all atoms are free of constraints, were used as the coordinates for the "reactant" state. The respective "product" state of the C2-flip was generated by swapping the coordinates of the two hydrogens (H_1 and H_2) of the rotating water molecule (a buried water in the case of ice and water W122 in the case of BPTI).

Reaction Path. The reactant and product conformers were provided as the two end points of the reaction path, which was calculated by the method of conjugate peak refinement (CPR),[18] using the default settings obtained when the "SADDLE" keyword is given in the TRAVEL module of the program CHARMM. The CPR algorithm finds the minimum-energy path in the form of a chain of conformers that follow a valley of the high-dimensional energy surface. It was run until convergence, at which point it has isolated those saddle points of the energy surface that are the transition states of the reaction. The use of the CPR method ensures that all degrees of freedom of the moving atoms (i.e., all atoms in the present study) are treated equally and avoids the bias that would result from the a priori choice of a constraining reaction coordinate.[29] The resulting CPR paths were smoothed by 500 cycles of synchronous chain minimization (SCM),[30,31] during which CPR was rerun every 100 SCM cycles to refine minor saddle point(s). This yields the energy profile $E(\lambda_\mu)$ along the intrinsic reaction coordinate λ_μ, which measures the progress of the reaction. λ_μ is the integral along the minimum energy path of the conformational changes occurring during the reaction. It is calculated by taking the sum (up to a given point n of the path) of the mass-weighted difference in coordinates ($\mathbf{r}_k$) between successive pairs of path points

$$\lambda_\mu = \sum_{k=1}^{n} |\mathbf{M}^{1/2}(\mathbf{r}_{k+1} - \mathbf{r}_k)| \tag{1}$$

where the matrix elements of $\mathbf{M}^{1/2}$ are $\delta_{ij}\sqrt{m_i}$ (m_i is the mass of atom i; δ_{ij} is 1 if $i = j$ and 0 if $i \neq j$). λ_μ is called λ when it is computed without mass weighting (i.e., all $m_i = 1$) and normalized so that $\lambda = 1$ represents the product of the reaction.

Vibrational Analysis and Kinetic Parameters. The gradient of the energy at a saddle point found by CPR is vanishing ($\sim 10^{-6}$ kcal mol^{-1} Å^{-1}), so that the normal modes of vibration at the transition state were calculated in the same manner as usually done in the reactant conformation, by diagonalizing the mass-weighted matrix of the second derivatives of the energy.[21] The square root of the resulting n eigenvalues, where n ($=3N - 6$) is the number of internal degrees of freedom, yields the normal-mode frequencies:[32] $\nu_i^{®}$ in the reactant and $\nu_i^{\dagger}$ at the TS ($i = 1 \rightarrow n$), where $\nu_1^{\dagger}$ is the single unstable (i.e., imaginary) frequency. Neglecting anharmonic effects, the reaction rate k was calculated with[33]

$$\mathrm{k} = \kappa \frac{kT}{h} \frac{Q_{\mathrm{vib}}^{\dagger}}{Q_{\mathrm{vib}}^{®}} \mathrm{e}^{-\beta \Delta E^{\dagger}} \tag{2}$$

where κ is the transmission coefficient correcting for deviations from transition-state theory (taken here as $\kappa = 1$), k is the Boltzmann factor ($\beta \equiv 1/kT$), and h is Plank's constant. $Q_{\mathrm{vib}}^{®}$ is the vibrational partition function of the reactant well. $Q_{\mathrm{vib}}^{\dagger}$ is the partition function at the barrier, excluding the degree of freedom of motion along the reaction coordinate. The translational partition function is invariant during the reaction and the rotational partition function is unaffected in the present case (the changes in the inertia tensor of the protein are negligible), so both functions can be ignored in eq 2. The canonical quantum partition function for each vibration mode ν is[34]

$$q_{\mathrm{vib}} = \frac{\mathrm{e}^{-\beta h\nu/2}}{(1 - \mathrm{e}^{-\beta h\nu})} \tag{3}$$

so that eq 2 can be rewritten as

$$\mathrm{k} = A \cdot \mathrm{e}^{-\beta(\Delta E^{\dagger} + \Delta Z^{\dagger})} \tag{4}$$

where the pre-exponential factor A is

$$A(n) = \frac{kT}{h} \frac{\prod_{i=1}^{n}(1 - \mathrm{e}^{-\beta h\nu_i^{®}})}{\prod_{i=2}^{n}(1 - \mathrm{e}^{-\beta h\nu_i^{\dagger}})} \tag{5}$$

and $\Delta Z^{\dagger}$ is the change in the zero-point energy between the reactant and the transition state:

$$\Delta Z^{\dagger} = \sum_{i=2}^{n}(1/2)h\nu_i^{\dagger} - \sum_{i=1}^{n}(1/2)h\nu_i^{®} \tag{6}$$

For small frequencies ($\nu_i < kT/h$), eq 5 reduces to the classical (high-temperature) limit:

$$A(n) \cong \frac{\prod_{i=1}^{n}\nu_i^{®}}{\prod_{i=2}^{n}\nu_i^{\dagger}} \tag{7}$$

The rate can also be expressed as

$$\mathrm{k} = w\, \mathrm{e}^{-\beta \Delta G^{\dagger}} \tag{8}$$

where w is the oscillation frequency in the reactant well for a motion that climbs to the TS along the curvilinear reaction coordinate λ_μ. $\Delta G^{\dagger} = \Delta E^{\dagger} + \Delta Z^{\dagger} + p\Delta V^{\dagger} - \mathrm{T}\Delta S^{\dagger}$ is the Gibbs free energy of activation. The amount of work $p\Delta V^{\dagger}$ in the reaction is negligible, so that combining eqs 4 and 8 gives an expression for the entropy of activation:

$$\Delta S^{\dagger}(w) = k \ln(A/w) \tag{9}$$

If the frictional/inertial effects leading to deviations from the minimum-energy path are ignored,[35] the well frequency w can be derived from the energy profile by fitting $E(\lambda_\mu)$ around the local minimum of the reactant with a simple functional $f(\lambda_\mu)$, for which the oscillation period is known.

Results

Ice. *Ground and Transition States.* In ice Ih (see Figure 1a), each water molecule makes four H-bonds to four neighboring water molecules (two H-bonds are donated and two are accepted) and is surrounded by several water molecules that form so-called L-defects. An L-defect is a pair of neighboring oxygen atoms with no protons in between them, for example, the water labeled LD in Figure 1.[20] The minimum-energy path

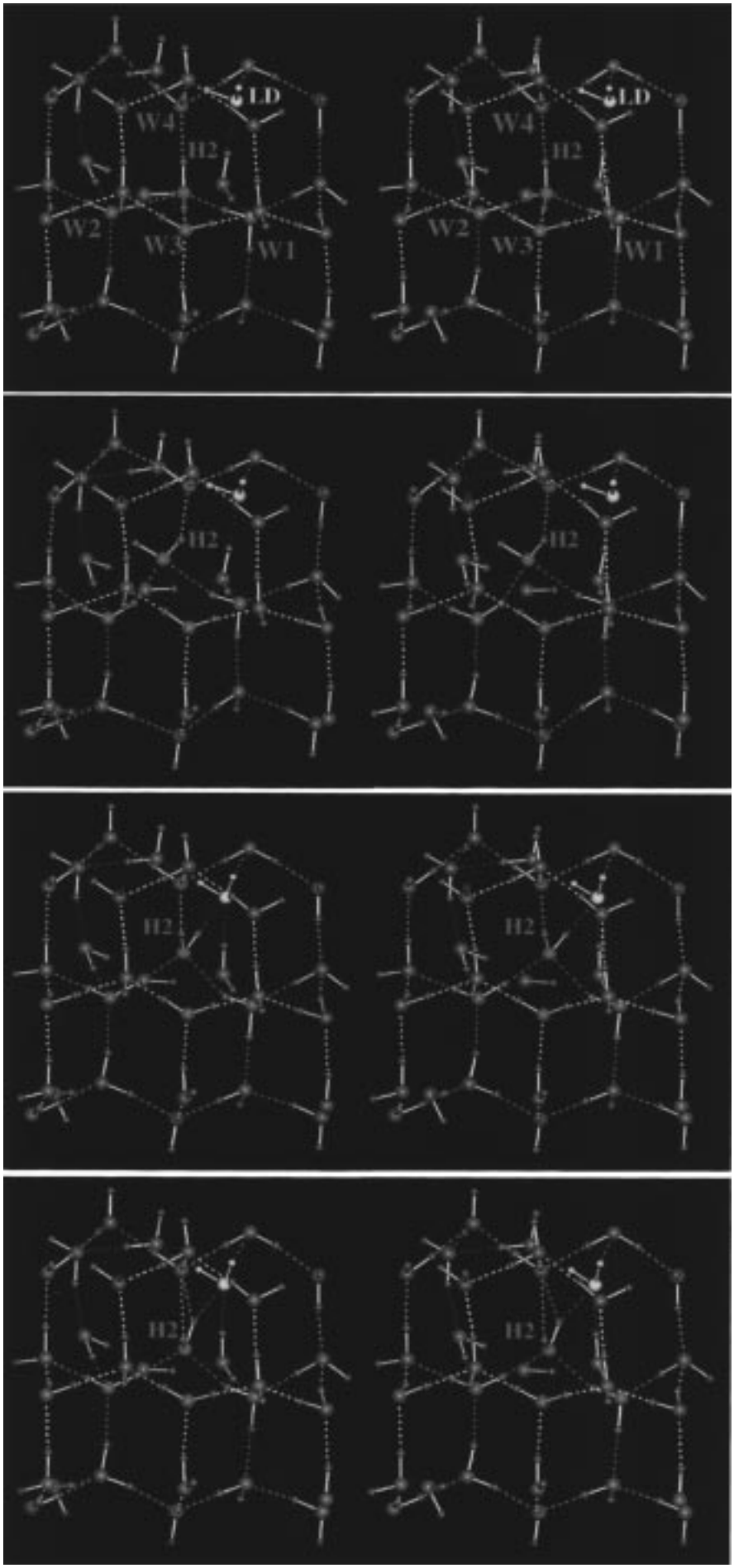

Figure 1. Kinematics of the C2-flip of water in ice Ih. The rotating water (WAT) is shown in red; its hydrogens are called H_1 and H_2. The stereoviews are taken at successive stages of the reaction (see the Methods section for a description of the intrinsic reaction coordinate λ): (a, top) the reactant ground state (GS) at $\lambda = 0.0$, $\alpha = 0°$; (b, top middle) the major transition state (TS) at $\lambda = 0.33$, $\alpha = 95°$; (c, bottom middle) the intermediate at $\lambda = 0.61$, $\alpha = 111°$; (d, bottom) the minor TS at $\lambda = 0.67$, $\alpha = 133°$. The product GS at $\lambda = 1.0$, $\alpha = 180°$ is identical to (a), except that H_1 and H_2 are interchanged. α is the angle between the vector joining H_1 to H_2 and the corresponding vector in the reactant GS orientation of WAT. The four water molecules making H-bonds with WAT are shown in green and are labeled W1, W2, W3, and W4 (see text). H_1 and H_2 are accepted by water molecules W3 and W4, while water molecules W1 and W2 each give one of their protons to the oxygen of WAT. The water molecule forming an L-defect with WAT is shown in yellow and labeled LD.

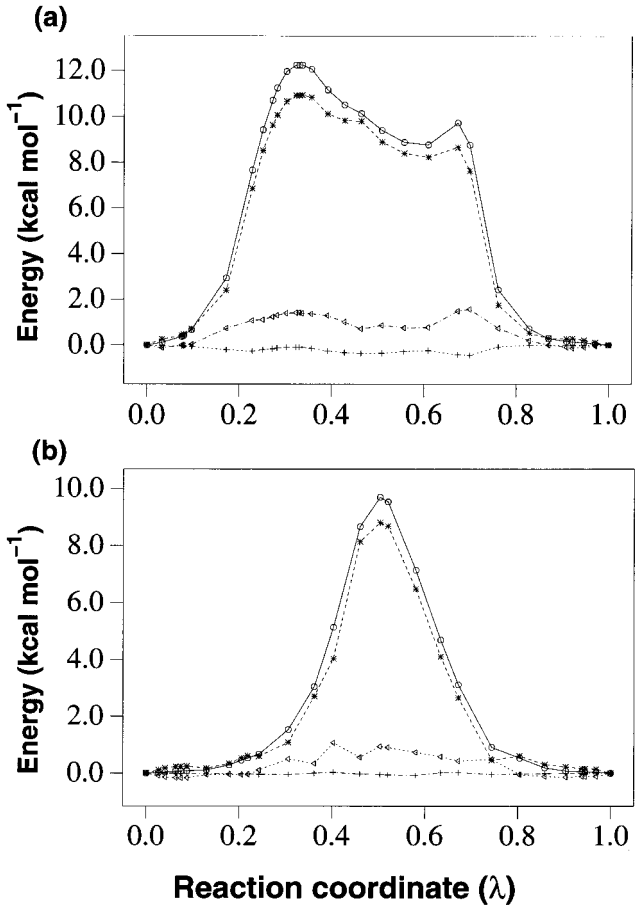

Figure 2. Potential energy profiles along the reaction path for the C2-flip of (a) a water molecule in ice Ih; (b) water W122 in BPTI. The intrinsic reaction coordinate λ is defined in the Methods section. $\lambda = 0$ represents the water molecule in the reactant state, and $\lambda = 1$ represents the product state, in which the positions of the two hydrogen atoms of the rotating water are interchanged. The total energy (○) is shown along with its three components: (+) the self-energy of the rotating water molecule (WAT); (△) the self-energy of the rest of the system (REST, i.e., all molecules except WAT); (*) the interaction energy between WAT and REST.

for the rotation of a given water molecule (hereafter WAT), leading to the interchange of its two hydrogen atoms (referred to as H_1 and H_2), was computed by the CPR method. The energy profile of this reaction, which we call the C2-flip, is plotted in Figure 2a. It shows a major transition state (TS) located one-third into the reaction, at $\lambda = 0.33$. Comparing its structure (see Figure 1b) to that of the ground state (GS) shows that WAT has moved by 1.1 Å, while water molecules in the first shell around WAT move by 0.3−0.5 Å; beyond this layer, the displacements induced by the rotation are less than 0.2 Å. The H_1-H_2 vector and the dipole moment vector make angles of 95° and 39° with respect to their GS orientations.

Activation Energy. The total energy barrier at the major TS is $\Delta E^{\dagger} = 12.3$ kcal mol^{-1}. This can be split into three components: the self-energy of WAT, the self-energy of the remaining water molecules, and the noncovalent interaction energy between WAT and the remaining water molecules, which are also plotted in Figure 2a. From Table 1, it can be seen that most of the activation energy is due to a deterioration of the interaction component, while both self-energy terms contribute little to the barrier. This reflects the fact that the H-bond network of the remaining water molecules is not modified by the rotation (see Figure 1). Only the H-bond made between H_1 and water W3 is broken at the TS, leaving H_1 "orphaned".

TABLE 1: Contributions to the Activation Energy[a] of the C2-Flip of Water in Ice-Ih and BPTI

	ice	BPTI
	Energies (kcal/mol)	
experimental E_a[b]	12.8 ± 0.9	na
computed $\Delta E^{\dagger}$	12.3	9.7
	Self-Energies[c]	
WAT	−0.1	−0.04
REST	1.43	0.94
	Interaction Energies[c]	
WAT-REST	10.93	8.80

[a] For each listed energy term, the activation energy $\Delta E^{\dagger}$ is the difference between the values of this term in the TS and GS. [b] Arrhenius activation energy.[20] [c] The computed $\Delta E^{\dagger}$ is decomposed into its three components: the self-energy of the rotating water WAT (for BPTI, WAT refers to W122), the self-energy of the rest of the system (REST), and the interaction energy between WAT and REST.

The H-bonds of WAT to its other three partners are maintained (with changes in the H-bond distance of less than 0.15 Å). Most of the destabilization at the TS (7 kcal mol^{-1}) is due to the loss of this one H-bond. The calculated barrier height is close to the Arrhenius activation energy reported experimentally at 12.8 ± 0.9 kcal mol^{-1}.[20] This good agreement suggests that the force-field and the computational methods employed are adequate to study the rotational isomerization of structural water.

Kinematics. As the reaction proceeds along the path, a weak H-bond is formed between the orphaned H_1 and water LD (see Figure 1c), yielding a shallow energy minimum 8.7 kcal mol^{-1} above GS at $\lambda = 0.6$ (Figure 2a). Further rotation breaks this intermediate H-bond as H_1 leaves LD to move toward W4 while H_2 leaves W4 to move toward W3. This results in a second (minor) TS at $\lambda = 0.67$ (Figure 2a), whose energy is 9.74 kcal mol^{-1} above GS. In this conformation (Figure 1d), H_1 and H_2 transiently make H-bonds to the same water (W3). This is the stage of the reaction at which the two hydrogens H_1 and H_2 actually switch their roles in the H-bond network. The H_1-H_2 vector and the dipole moment vector are oriented at 133° and 44° with respect to their GS orientations. Finally, the reaction ends ($\lambda = 1.0$) with the system going into the product GS, which is identical to the reactant GS (Figure 1a), except for the interchange of H_1 and H_2. During the whole reaction, the oxygen of WAT maintains its two H-bonds with water molecules W1 and W2 (see Figure 1a−d). The motion is not a simple rotation around the C2-symmetry axis of WAT but involves two distinct types of motion that occur sequentially. In the first part of the reaction ($\lambda = 0.0 \rightarrow 0.6$), H_1 rotates by half a turn around an axis defined by the $O-H_2$ bond, whose orientation is maintained by the H-bond with water W4. During the second part of the reaction ($\lambda = 0.6 \rightarrow 1.0$), the motion becomes an in-plane rotation, which completes the C2-flip. This two-step process is schematically shown in Figure 3b. It is in the second step that the H-bond with water W4 switches from H_1 to H_2.

Randomness of Hydrogen Placement. To investigate the dependence of the energy barrier on disorder in the local ice environment, we used a unit cell (of 96 water molecules) kindly supplied by Prof. J. Reimers, which has randomness in the hydrogen bonding so that the overall dipole moment of the cell is zero.[36] A nonperiodic box of dimension 37 × 31 × 29 Å was build of 8 such cells (for a total of 768 molecules) and subjected to orthorhombic periodic boundary conditions. Rather than generating different boxes with random hydrogen placement, we looked instead at different water molecules in this box, each molecule having a different local environment. The rotation paths for 18 water molecules were calculated (data not

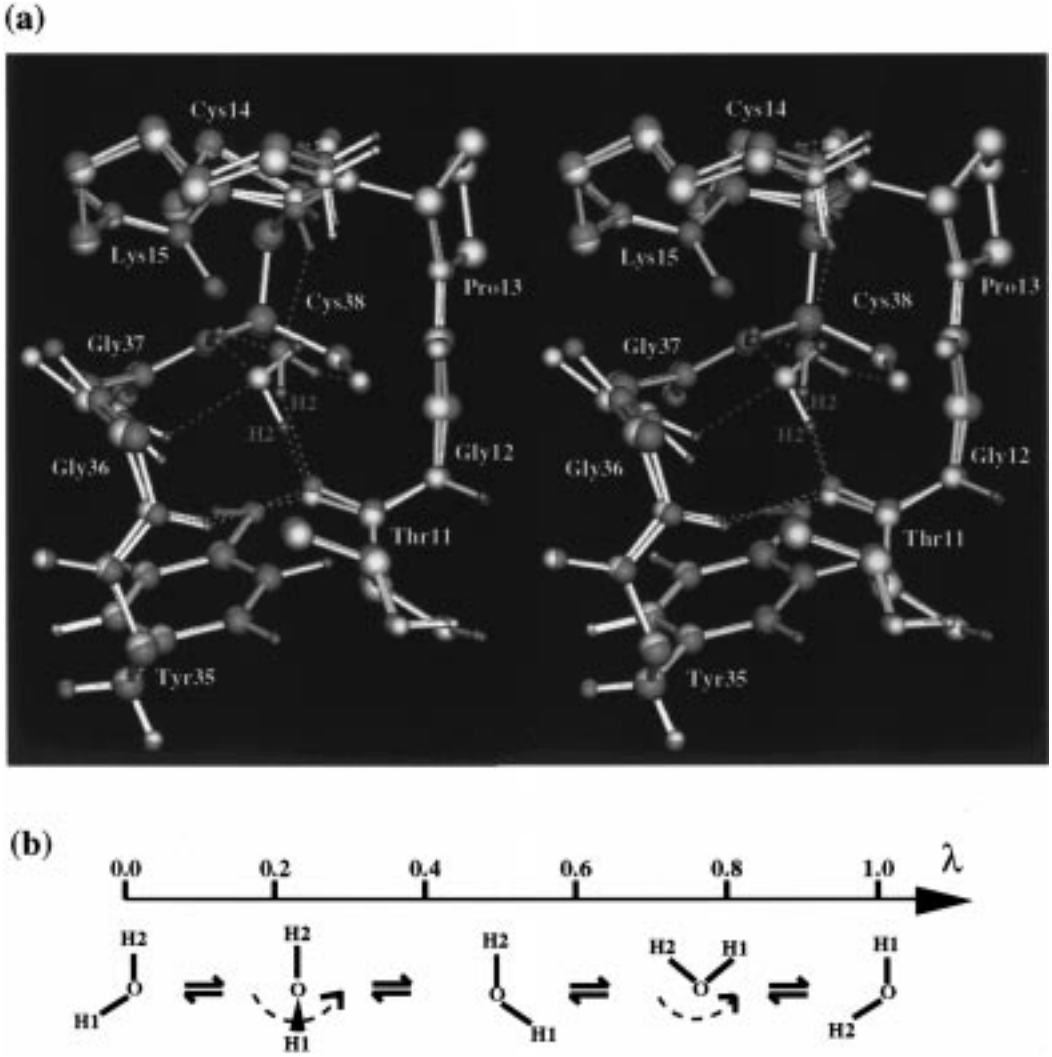

Figure 3. (a) Stereoviews of the ground (GS) and transition state (TS) of the reaction path for the C2-flip of water W122 in BPTI. The GS structure ($\lambda = 0.0$, $\alpha = 0°$) is in red, with its hydrogens in green. The TS structure ($\lambda = 0.5$, $\alpha = 95°$) is in yellow, with its hydrogens in blue. Proton H_2 of water W122 is labeled. See caption of Figure 1 for the definition of α. (b) Sequence of events for the C2-flip of a water molecule in ice and of water W122 in BPTI (see text). λ is the reaction coordinate described in Methods. Rotating motion is depicted by curly arrows in broken line. As shown here ($\lambda = 0 \rightarrow 1$), the water molecule rotates around the O−H_2 bond during the first half of the reaction and rotates in its own plane during the second half. Following the principle of microscopic reversibility, the reverse order of events ($\lambda = 1 \rightarrow 0$) is just as likely. In either direction of the reaction, the outcome is the interchange of the two hydrogens H_1 and H_2.

shown). The resulting activation barriers range from 9.7 to 11.0 kcal mol^{-1}, with an average of 10.5 kcal mol^{-1} and a standard deviation of 0.5 kcal mol^{-1}. For all these paths, the energy profile displays a major and a minor TS and the motion of the rotating water is a two-step process as described above.

BPTI. *Ground and Transition States.* This section describes the reaction path computed for the C2-flip of a structural water (number W122) in BPTI. We refer to the two hydrogens of W122 as H_1 and H_2. In the reactant GS, W122 accepts two and donates two H-bonds: the oxygen of W122 is H-bonded to the N−H groups of Cys14 and Cys38, while H_1 is H-bonded to the C═O group of Cys38 and H_2 is H-bonded to the C═O group of Thr11 (see Figure 3a). The product GS is identical to the reactant structure, except for the interchange of the two hydrogens H_1 and H_2. Figure 2b shows the energy profile along the minimum-energy path joining the reactant to the product conformers obtained by CPR. The reaction has a single TS at $\lambda = 0.5$, whose structure is shown overlaid onto the reactant GS in Figure 3a. In the TS conformation, the plane holding the three atoms of W122 is almost perpendicular to the corresponding plane in the GS. The H_1-H_2 vector and the dipole moment vector make angles of 95° and 49° relative to their respective directions in the GS. The oxygen atom of W122 is located 0.6 Å from its GS position. The rmsd between GS and TS for the whole system is only 0.09 Å. The principal perturbation of the protein is a partial rotation of two peptide planes, $CO_{Gly36}-NH_{Gly37}$ and $CO_{Pro13}-NH_{Cys14}$, by 10° and 20°, respectively. The peptide proton of Cys14 is displaced by 0.6 Å, and the 35−38 loop moves away from water W122 by 0.1−0.3 Å. Residues farther than 6 Å from water W122 undergo displacements smaller than 0.1 Å.

Activation Energy. The potential energy barrier of the C2-flip is 9.7 kcal mol^{-1}, most of which (8.8 kcal mol^{-1}) arises from a deterioration of water/protein interactions (see Table 1; Figure 2b). The disruption of the protein contributes only 0.94 kcal mol^{-1} to the barrier, while water W122 undergoes no strain at all. The changes in the H-bond network at the TS are slightly more complicated than described above in the case of ice. Two of the four GS H-bonds between the protein and W122 are broken at the TS (one with the acceptor $C=O_{Cys38}$ and the other with the donor NH_{Cys14}), while a transient H-bond is formed with NH_{Gly37} as donor (see Figure 3a). As a result, a total of 3 H-bonds between the protein and W122 are present in the TS, so that the net change in the number of H-bonds relative to the

TABLE 2: Largest Residuewise Contributions (in kcal mol^{-1}) to the Activation Energy of the Water-Flip in BPTI[a]

residue	interaction energy	elec.	vdW
Cys14	3.80	4.57	−0.77
Cys38	3.49	4.19	−0.70
Thr11	2.08	1.79	0.29
Gly12	1.60	2.01	−0.41
Pro13	1.18	0.95	0.23
Lys15	0.65	0.65	0.00
Arg39	0.32	0.28	0.04
Gly36	−1.91	−2.42	0.51
Gly37	−2.33	−3.45	1.12
total	8.88	8.57	0.31

[a] The interaction energy is split into its electrostatic (elec.) and van der Waals (vdW) components.

GS is −1. This accounts for a barrier height similar in value to the one computed for ice, since in both cases at most one H-bond is lost during the C2-flip. The principal interactions between W122 and single protein residues are listed in Table 2. Destabilization of the TS is mostly due to the loss of the H-bond of W122 with CO_{Cys38} and to the unfavorable orientation of H_1 with respect to NH_{Cys14} (see Figure 3a). The formation of the H-bond between WAT and NH_{Gly37} stabilizes the TS by 2.33 kcal mol^{-1} while interactions with Gly36 further stabilize the TS by 1.9 kcal mol^{-1}.

We investigated the dependence of the energy barrier in BPTI on solution and on conformational fluctuations of the protein. For this purpose, the protein was placed inside a sphere (diameter 30 Å) of water molecules and subjected to molecular dynamics at 300 K. Structures taken at successive stages along the simulation were quenched. For each of these solvated conformations, the rotation path of W122 was recalculated (data not shown). The resulting activation barriers were all within 0.6 kcal mol^{-1} of the one reported above. This shows that the process is governed by short-range interactions with the well-packed protein interior and is little affected by solvent.

Kinematics. Although the energy profiles for ice and BPTI are different, the motion of the rotating water in BPTI is essentially the same as in ice: rotation occurs sequentially around two distinct axes (see Figure 3b), starting ($\lambda = 0.0 \rightarrow 0.5$) with a rotation of W122 around its O−H_2 bond, whose orientation is maintained by the H-bond between H_2 and Thr11, and ending ($\lambda = 0.5 \rightarrow 1.0$) with an in-plane rotation, during which the H-bond with Thr11 switches from H_2 to H_1.

Vibrational Analysis. A normal-mode analysis was performed on the reactant and on the TS conformations of BPTI/W122. At the TS, a single unstable mode was found, as expected for a nondegenerate saddle point. Its imaginary frequency $\nu_1^{\dagger}$ is 380 cm^{-1}. The motion resulting from a small displacement along this eigenvector is the rotation of H_1 (by 10° at 300 K) around the axis of the O−H_2 bond in W122; all other atoms remain essentially immobile along this mode. The stable modes ν_i of the TS ($i = 2 \rightarrow 2466$) and of the reactant conformation ($i = 1 \rightarrow 2466$) are shown in Figure 4a. The lowest-mode frequency is 6.9 and 6.5 cm^{-1} in the reactant and at the TS, respectively. Starting at mode number 2165, the frequency jumps to high frequencies (≥2889 cm^{-1}). These correspond to the bond vibrations of the 302 hydrogen atoms present in the system. From Figure 4a, it can be seen that the frequencies of the modes in the reactant well and at the TS are very similar, with the differences between closest pairs of frequencies not exceeding 5.9% and only 0.13% on average. Yet, these small differences are responsible for a non-negligible vibrational entropy of activation (discussed below).

Rate Factor. The effect on the reaction rate of the above mentioned changes in the vibrational spectrum is contained in the pre-exponential rate factor A of eq 4 (see Methods section). The entropy of activation also covaries directly with A (eq 9). Figure 4b shows the evolution of $A(n)$ as progressively more modes are included. Both the quantum (eq 5) and the classical value (eq 7) are plotted. Both curves reach a plateau at mode number 1100, whose frequency is 620 cm^{-1}. This shows that only modes with frequencies smaller than 620 cm^{-1} contribute to the difference in vibrational entropy between the reactant and the TS. These frequencies are much lower than those of the three vibration modes of an isolated water molecule (1737, 3323, and 3370 cm^{-1}, calculated with the energy function used here for water). This indicates that the modified modes at the TS are not the internal modes of water W122 but are more collective vibration modes involving the protein cage around W122. The part of the vibrational spectrum contributing to the activation entropy is similar to the one found to contribute to the entropy of dimerization for insulin, which involves frequencies up to 600 cm^{-1}.[37] The classical and quantum expressions for $A(n)$ diverge significantly above the 100th mode (48 cm^{-1}). This is not surprising, since at 300 K $kT/h = 208.4$ cm^{-1} and the classical limit of eq 7 is only valid for frequencies well below that value. Because more than half of the modes that contribute to the vibrational entropy of activation have a frequency larger than kT/h, it is not adequate to use the classical limit to evaluate the reaction rate. The height of the plateau in Figure 4b ($A_{quantum} = 1528.4$ cm^{-1} and $A_{classical} = 6120.1$ cm^{-1} when all modes are included) is much higher than the frequency at which the plateau is reached (620 cm^{-1}). This shows that the value of A is not merely due to the excess of one mode in the reactant but that A is dominated by the accumulation over

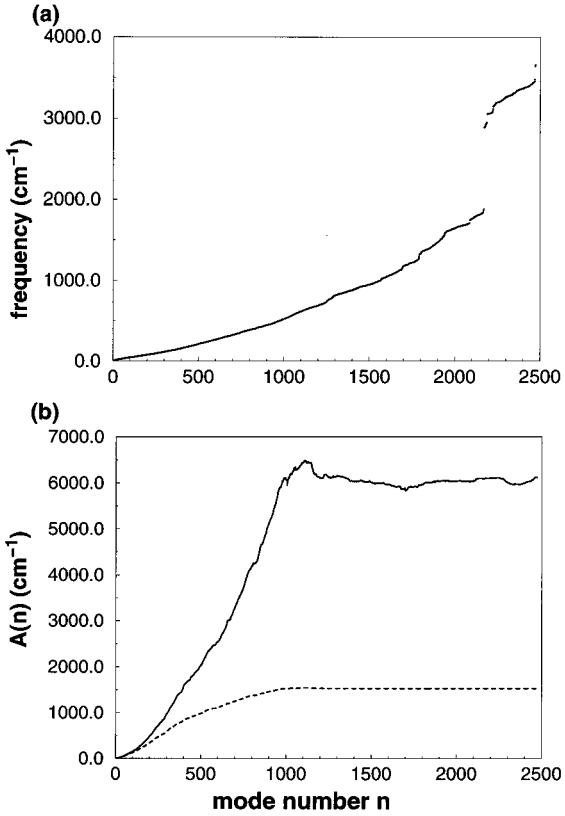

Figure 4. (a) Vibration frequencies of the normal modes calculated in the GS and at the TS for the rotation of water W122 in BPTI (the two curves are indistinguishable on this frequency scale, see text). To get a view of the cumulative density of states (not normalized), rotate the plot counterclockwise by 90°. (b) Pre-exponential rate factor $A(n)$ for the quantum (- - -) and the classical (—) case, at 300 K (see eqs 5 and 7 in the Methods section).

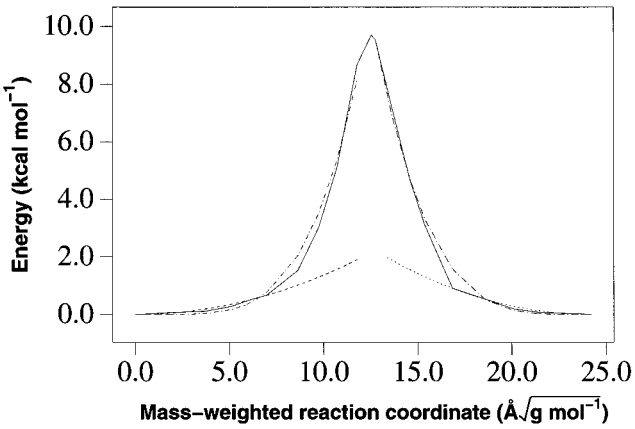

Figure 5. Energy profile $E(\lambda_\mu)$ (—) for the rotation of water W122 in BPTI. The mass-weighted reaction coordinate λ_μ is described in the Methods section (eq 1). The reactant and product wells have been fitted either with a quadratic function (- - -) or with a quartic function (— · —), to derive a value for the well frequency w (see text).

the first 1100 modes of the minute frequency differences in each mode between the reactant and TS.

Well Frequency. To extract the activation entropy $\Delta S^\dagger$ from the pre-exponential factor A, it is necessary to assign a value to the well-frequency w (see eq 9). Figure 5 shows that the low-energy regions ($E \leq 1$ kcal mol^{-1}) of the energy profile $E(\lambda_\mu)$ can be fitted by a quadratic function $f(\lambda_\mu) = (1/2)k_H\lambda_\mu^2$. The fit gives $k_H = 27$ cal (Å^2 g)$^{-1}$ in the reactant and $k_H = 33$ cal (Å^2 g)$^{-1}$ in the product. Since $w = \sqrt{k_H}$, this yields well frequencies w of 18 cm^{-1} for the reactant and 20 cm^{-1} for the product well. For oscillations to higher energy levels, a quartic function of the form $f(\lambda_\mu) = k_Q\lambda_\mu^4$ provides a better fit in the present case, with $k_Q = 0.6$ mcal·mol (Å^4·g^2)$^{-1}$ for both the reactant and product well. The corresponding frequency was derived numerically to be $w = 42$ cm^{-1} for an oscillation with a maximum potential energy increase $\Delta E = 4$ kcal mol^{-1} or $w = 50$ cm^{-1} for $\Delta E = 9$ kcal mol^{-1}.

We found that it is not adequate to get the well frequency from a projection of the unstable eigenvector of the TS (the mode corresponding to $\nu_1^\dagger$) onto the eigenvectors of the reactant. Indeed, atomic displacements from the GS conformation taken along the direction of the unstable mode occur with an oscillation frequency of 968 cm^{-1}, which is too high to correspond to the libration of a water molecule in a cavity. Because the reaction path of a rotation is very curved when it is expressed in Cartesian coordinates, the unstable eigenvector corresponding to a rigid-body rotation of W122 in the TS orientation results in the distortion of this same W122 in the GS orientation. This explains the high frequency obtained.

Discussion

Comparing BPTI with Ice. The mechanism for water rotation by C2-flip is similar in the cases of ice and BPTI/W122. In both systems, the motion of the rotating water sequentially involves two distinct rotation axes (Figure 3b). As a result the orientation of the dipole vector of the rotating water changes significantly (62° in ice and 49° in BPTI), which would not be the case if the flip involved only a rotation around the C2 axis of symmetry. The first partial rotation is a half-turn around the O—H_2 bond (where H_2 is defined as the hydrogen of the rotating water that maintains its H-bond), during which H_1 becomes an "orphaned" H-bond donor. This is followed by a rotation around an axis orthogonal to the plane of the water molecule (i.e., in-plane rotation), during which H_1 takes the place of H_2. When the H-bond acceptor switches from H_2 to H_1 in this second phase, a bifurcated H-bond is formed transiently (see Figure 1d in the case of ice). Stable bifurcated H-bonds, which can be found in proteins[38,39] and in crystal hydrates,[40] are believed to increase the mobility of water molecules by providing low-energy paths between conformations with different tetrahedral arrangements of H-bonds.[40]

The difference in the barrier height of the C2-flip between ice and BPTI, i.e. 12.3 and 9.7 kcal mol^{-1} respectively, is due to the different environments of H-bond donors around the rotating water molecule. In ice, all H-bond donors surrounding the rotating water are "sequestered" by strong H-bonds to other water molecules, so that the oxygen of the rotating water is obliged to interact with the same two H-bond donors as in the GS. In the case of BPTI, the rotating water can compete for another H-bond donor, which is involved in a weak interaction with the protein in the GS. Indeed, the amide proton NH_{Gly37} (located near W122) makes a favorable interaction with the π-orbitals of the phenyl ring of Tyr35 (this interaction is modeled in the present calculation by the interaction with the electrostatic quadrupole of the phenyl ring). During rotation, this interaction is replaced by the stronger H-bond that NH_{Gly37} can make with the oxygen of W122, since this oxygen has lost one of its coordinating H-bond donors (NH_{Cys14}, see Figure 3a). This ability of the water oxygen to hop from one H-bond donor (NH_{Cys14}) to another (NH_{Gly37}) breaks the tetrahedral symmetry in the local potential energy surface around the water molecule[41] and gives an extra degree of freedom to W122 in BPTI, which is responsible for the lower energy barrier in BPTI. The proposed reorientation of the NH_{Gly37} bond is consistent with the observation that the NH bond vector of Gly37 displays the lowest order parameter among all NH bond vectors surrounding W122.[42]

Entropy of Activation and Reaction Rate. Differences in the vibrational entropy between stable conformations of a protein have been calculated, for instance, in the dimerization of insulins.[37] The normal-mode analysis underlying such calculations requires that the conformers have a vanishing energy gradient.[21] While finding a local energy minimum is routine even in large systems, the stationary point corresponding to the transition state of a reaction could not be reliably determined so far for systems as large as a macromolecule. For this reason, the calculation of the vibrational entropy difference relative to the transition state of a reaction had never been performed for a protein. Because the CPR algorithm finds the actual saddle point(s) as one of the conformers along the reaction path, a normal-mode analysis at the TS for the rotation of W122 in BPTI was possible. The resulting vibration frequencies can then be used to compute the pre-exponential rate factor A (see above).

Once A has been determined, the calculation of the activation entropy still requires the choice of an appropriate value for the well frequency w (see eq 9). The frequencies from the quartic fit (see Results) better describe the motion of a molecule having acquired the needed activation energy and about to go over the barrier, so that they would be suitable for use in eq 8 if $\Delta G^\dagger$ was already known. But in eq 9, we use w to actually extract $\Delta S^\dagger$ from A, which relies on a harmonic expansion of the energy function in the reactant well in terms of the frequencies $\nu_i^{\circledR}$ (eq 5). Therefore, it is more consistent to use a value for w that was also obtained by harmonic expansion in the well (i.e., the quadratic fit). Using $w = 20$ cm^{-1} and $A_{quantum} = 1528.4$ cm^{-1} yields a vibrational activation entropy contribution $T\Delta S^\dagger = +2.58$ kcal mol^{-1} (at 300 K). This positive entropy change means that there is more "disorder" in the TS of the BPTI/

TABLE 3: Summary of the Kinetic Parameters for the Rotation of Water W122 in BPTI, at 300 K[a]

$A_{quantum}$	1528.4 cm^{-1}
w	20 cm^{-1}
$\tau = 1/k$	45 ns
$-T\Delta S^{\dagger}$ (w)	−2.58 kcal mol^{-1}
$\Delta E^{\dagger}$	9.7 kcal mol^{-1}
$\Delta Z^{\dagger}$	−1.04 kcal mol^{-1}
$\Delta G^{\dagger}$ (w)	6.08 kcal mol^{-1}

[a] See Methods section for definitions.

W122 complex than in the GS. This is consistent with our finding that the H-bond network is looser at the TS, with W122 making one less H-bond than in the GS. Our estimate of the vibrational entropy could be improved by accounting for the effects of anharmonicity that result at high temperatures. This can be done by a quasi-harmonic analysis[43] of trajectories generated through molecular dynamics simulations. This approach would be relatively straightforward in the case of the stable GS, but it is very difficult to constrain the dynamics in the vicinity of the TS.[24]

Applying eq 4 with the kinetic parameters summarized in Table 3 gives a rotation time for the C2-flip of W122 in BPTI of $\tau \equiv 1/k = 45$ ns. This value of τ must be considered as a lower bound, since the actual transmission coefficient κ could be slightly smaller than 1.0.[35] It is not very much longer than the rotational correlation time of the protein, measured to be 9.7 ns at 27 °C.[13] Thus in the context of NMRD experiments, one must be careful when assuming that structural water is fully "immobilized" inside a protein. Note that if the changes in the vibrational spectrum had been ignored (i.e., if the pre-exponential factor A had been defined as kT/h), then the rotation time would have become $\tau = 1.9$ μs. This shows that the contribution of the vibrational entropy to the reaction rate can be significant.

Meaning of the Activation Entropy. The dependence of the activation entropy on the well frequency w (eq 9) leads to an interesting question about the nature of an activation entropy. For example, in the case of water rotation in BPTI, the factor A (eq 5) takes the same value whether one considers the forward or the reverse reaction, since the n vibration frequencies $\nu_i^{\ddagger}$ are identical in the reactant and the product conformations. For the same reason, the vibrational entropy of the reactant (S_r) is equal to that of the product (S_p):

$$S_r = S_p \tag{10}$$

The activation entropy can be written for the forward reaction as

$$\Delta S^{\dagger}(w_{\rightarrow}) \equiv S^{\dagger}_{\rightarrow} - S_r \tag{11}$$

or for the reverse reaction as

$$\Delta S^{\dagger}(w_{\leftarrow}) \equiv S^{\dagger}_{\leftarrow} - S_p \tag{12}$$

We have shown that the oscillating motion that leads to the TS is different on the reactant side (rotation around the $O-H_2$ bond) than on the product side (in-plane rotation, see Figure 3b), so that w is different for the forward ($w_{\rightarrow}$) and reverse ($w_{\leftarrow}$) reactions. Therefore, applying eq 9 gives an entropy of activation that is different for the forward and the reverse reaction

$$\Delta S^{\dagger}(w_{\rightarrow}) \neq \Delta S^{\dagger}(w_{\leftarrow}) \tag{13}$$

Combining the last equation with eqs 10−12, one obtains

$$S^{\dagger}_{\rightarrow} \neq S^{\dagger}_{\leftarrow} \tag{14}$$

This last equation says that the entropy at the transition state depends on whether it is calculated with respect to the forward or the reverse reaction. How can this be true, since entropy is a state function and should not depend on the path followed to reach the transition state? This false paradox arises because the entropy at a TS is not an intrinsically defined quantity (as it would be in a stable state) but requires the choice of a conformational subspace that contains the TS and separates the reactant from the product. Indeed, the entropy content of a TS would have to be calculated within this subspace, which can be viewed as a hypersurface (of dimension $n - 1$) "orthogonal" to the direction of the path. In the present example, a different motion on each side of the TS implies different path directions, which in turn define different hypersurfaces. Consequently, $S^{\dagger}_{\rightarrow}$ and $S^{\dagger}_{\leftarrow}$ are different in eq 14 because they are the entropies of two different dividing surfaces. In other words, the entropy of activation $\Delta S^{\dagger}$ is dependent on which surface is chosen to formally separate the reactant from the product. In eq 8, a change in the value of w is directly compensated by a change in $\Delta G^{\dagger}$ (through $\Delta S^{\dagger}$), so that the value of the rate k remains constant. More generally, a change in the free energy of activation due to a different choice of dividing surface is compensated by a change in the transmission coefficient,[44,45] so that the reaction rate is always independent of this choice. On the other hand, it is important to remember that an entropy of activation is dependent on the implicit or explicit choice of a reaction coordinate. A common example of such an implicit choice is when the well frequency w in eq 8 is replaced with the pre-exponential factor kT/h of Eyring's rate law, as is often done for the interpretation of measurements of the rate dependence on temperature. With $w \equiv kT/h = 208.4$ cm^{-1} at 300 K, the entropic contribution obtained from eq 9 would then be $T\Delta S^{\dagger} = 1.2$ kcal mol^{-1}, which is only about half the value obtained with $w = 20$ cm^{-1}. This exemplifies that the entropy of activation must be considered as a parameter of a chosen rate law rather than as an intrinsic thermodynamic quantity.

Choice of the Methodology. The capability of the CPR algorithm to find the intrinsic reaction coordinate of a reaction system was a prerequisite for the present study. The intrinsic reaction coordinate is the curvilinear path in conformational space that follows the deep "valleys" on the high-dimensional energy surface (on which the reactant and the product are local minima). It would not have been possible to find this minimum-energy path as done usually, i.e., by simply choosing some internal coordinate and performing energy minimizations with a varying constraint on that predefined reaction coordinate. Indeed, our results have shown that the unconstrained motion along the intrinsic reaction coordinate involves the sequential rotation of the water molecule around two orthogonal axes. This means that any a priori choice of a simple rotation axis (for example, the C2-symmetry axis of the rotating water) would not have been a suitable reaction coordinate. CPR allows the study of any type of reaction[46,47] and has been applied recently to another aspect of water mobility in proteins: the exchange of structural water molecules with bulk solvent.[48]

Exploring the Energy Surface. When considering the rotation of a water molecule, the symmetry of the molecule suggests three types of motion:[49] (1) a C2-flip around an axis corresponding to the C2-symmetry of the water molecule; (2) a pitch-flip around an axis parallel to the line joining the two hydrogen atoms of the water molecule; (3) an in-plane rotation, whose axis is orthogonal to the previous two axes. Only the

C2-flip results in the interchange of the two hydrogens of the water. We investigated whether the other two types of motion are relevant to the rotation of a structural water. The calculation of a reaction path involving either a full (360°) pitch-flip or a full in-plane rotation was attempted, since the CPR method enables the refinement of a specific path by starting from an initial guess path (defined by a series of conformations). For both kinds of motions, the resulting minimum-energy path was an essentially identical succession of two half-turns of the water molecule, each one involving the interchange of the water hydrogens (i.e., a C2-flip). This behavior was observed in both ice and BPTI. This means that a full turn by pitch-flip or by in-plane rotation does not correspond to a separate valley on the energy surface of ice or of BPTI. Only a path leading to the interchange of the two hydrogen atoms of the water follows a marked valley on the energy surface. For this reason, the present study could be limited to the C2-flip reaction.

Acknowledgment. We thank Prof. B. Halle for advice and preprints of his papers and Prof. G. Dodson, Dr. Leo Caves, and Prof. R. J. Wittebort for helpful comments. We are grateful to Prof. J. Reimers for the coordinates of the ice unit cell. C.S.V. thanks the BBSRC for support.

References and Notes

(1) Wuthrich, K. Hydration of biological macromolecules in solution—surface structure and molecular recognition. *Cold Spring Harbor Symp. Quant. Biol.* **1993**, *58*, 149−157.

(2) Denisov, V. P.; Halle, B. Protein hydration dynamics in aqueous solution. *Faraday Discuss.* **1996**, *103*, 227−244.

(3) Levitt, M.; Park, B. H. Water—now you see it, now you don't. *Structure* **1993**, *1*, 223−226.

(4) Brooks, C. L.; Karplus, M. Solvent effects on protein motion and protein effects on solvent motion-dynamics of the active site region of lysozyme. *J. Mol. Biol.* **1989**, *208*, 159−181.

(5) Daggett, V.; Levitt, M. Realistic simulations of native protein dynamics in solution and beyond. *Annu. Rev. Biophys. Biomol. Struct.* **1993**, *22*, 353−380.

(6) Brunne, R. M.; Liepinsh, E.; Otting, G.; Wuthrich, K.; vanGunsteren, W. F. Hydration of proteins-a comparison of experimental residence times of water molecules solvating the bovine pancreatic trypsin inhibitor with theoretical model calculations. *J. Mol. Biol.* **1993**, *231*, 1040−1048.

(7) Phillips, G. N.; Pettitt, B. M. Structure and dynamics of the water around myoglobin. *Protein Sci.* **1995**, *4*, 149−158.

(8) Abseher, R.; Schreiber, H.; Steinhauser, O. The influence of a protein on water dynamics in its vicinity investigated by molecular dynamics simulation. *Proteins: Struct., Funct., Genet.* **1996**, *25*, 366−378.

(9) Billeter, M.; Guntert, P.; Luginbuhl, P.; Wuthrich, K. Hydration and DNA recognition by homeodomains. *Cell* **1996**, *85*, 1057−1065.

(10) Tame, J. R. H.; Sleigh, S. H.; Wilkinson, A. J.; Ladbury, J. E. The role of water in sequence independent ligand binding by an oligopeptide transporter protein. *Nat. Struct. Biol.* **1996**, *3*, 998−1001.

(11) Otting, G.; Liepinsh, E.; Wuthrich, K. Protein hydration in aqueous solution. *Science* **1991**, *254*, 974−980.

(12) Ernst, J. A.; Clubb, R. T.; Zhou, H. X.; Gronenborn, A. M.; Clore, G. M. Demonstration of positionally disordered water within a protein hydrophobic cavity by NMR. *Science* **1995**, *267*, 1813−1817.

(13) Denisov, V. P.; Peters, J. Horlein, H. D.; Halle, B. Using buried water molecules to explore the energy landscape of proteins. *Nat. Struct. Biol.* **1996**, *3*, 505−509.

(14) Denisov, V. P.; Halle, B. Residence times of the buried water molecules in bovine pancreatic trypsin inhibitor and its G36S mutant. *Biochemistry* **1995**, *34*, 9046−9051.

(15) Denisov, V. P.; Halle, B. Protein hydration dynamics in aqueous solution—a comparison of bovine pancreatic trypsin inhibitor and ubiquitin by O-17 spin relaxation. *J. Mol. Biol.* **1995**, *245*, 682−697.

(16) Denisov, V. P.; Halle, B. Hydrogen exchange and protein hydration—the deuterium spin relaxation dispersions of bovine pancreatic trypsin inhibitor and ubiquitin. *J. Mol. Biol.* **1995**, *245*, 698−709.

(17) Wlodaver, A.; Walter, J. Huber, R.; Sjolin, L. Structure of Bovine pancreatic trypsin inhibitor. Results of joint neutron and X-ray refinement of crystal form II. *J. Mol. Biol.* **1984**, *180*, 301−329.

(18) Fischer, S.; Karplus, M. Conjugate Peak Refinement—an algorithm for finding reaction paths and accurate transition-states in systems with many degrees of freedom. *Chem. Phys. Lett.* **1992**, *194*, 252−261.

(19) Kuhs, W. F.; Lehmann, M. S. The structure of ice Ih by neutron diffraction. *J. Phys. Chem.* **1983**, *87*, 4312−4313.

(20) Wittebort, R. J.; Usha, M. G.; Ruben, D. J.; Wemmer, D. E.; Pines, A. Observation of molecular reorientation in ice by proton and deuterium magnetic resonance. *J. Am. Chem. Soc.* **1988**, *110*, 5668−5671.

(21) Brooks, B. R.; Janezic, D.; Karplus, M. Harmonic analysis of large systems. 1. Methodology. *J. Comput. Chem.* **1995**, *16*, 1522−1542.

(22) Brooks, B. R.; Bruccoleri, R. E.; Olafson, B. D.; States, D. J.; Swaminathan, S.; Karplus, M. CHARMM—a program for macromolecular energy, minimization and dynamics calculations. *J. Comput. Chem.* **1983**, *4*, 187−217.

(23) Jorgensen, W. L.; Chandrasekhar, J.; Madura, J. D.; Impey, R. W.; Klein, M. L. Comparison of simple potential functions for simulating liquid water. *J. Chem. Phys.* **1983**, *79*, 926−935.

(24) Neria, E.; Fischer, S.; Karplus, M. Simulation of activation free energies in molecular systems. *J. Chem. Phys.* **1996**, *105*, 1902−1921.

(25) Mackerell, A. D.; Bashford, D.; Bellott, M.; Dunbrack, R. L.; Field, M. J.; Fischer, S.; Gao, J.; Guo, H.; Ha, S.; Joseph, D.; Kuchnir, L.; Kuczera, K.; Lau, F. T. K.; Mattos, C.; Michnick, S.; Nguyen, D. T.; Ngo, T.; Prodhom, B.; Roux, B.; Schlenkrich, M.; Smith, J.; Stote, R.; Straub, J.; Wiorkiewiczkuczera, J.; Karplus, M. Self-consistent parameterization of biomolecules for molecular and condensed phase simulations *FASEB J.* **1992**, *6*, A143.

(26) Larsson, K.; Tegenfeldt, J.; Hermansson, K. Reorientation of water molecules in solid hydrates—correlation with spectroscopic and structural data. *J. Chem. Soc., Faraday Trans.* **1991**, *87*, 1193−1200.

(27) Bruccoleri, R. E.; Karplus, M. Spatially constrained minimization of macromolecules. *J. Comput. Chem.* **1986**, *7*, 165−175.

(28) Verma, C. S.; Fischer, S.; Caves, L. S. D.; Roberts, G. C. K.; Hubbard, R. E. Calculation of the reaction pathway for the aromatic ring flip in methotrexate complexed to dihydrofolate reductase. *J. Phys. Chem.* **1996**, *100*, 2510−2518.

(29) Fischer, S.; Dunbrack, R.; Karplus, M. Cis−trans imide isomerization of the proline dipeptide. *J. Am. Chem. Soc.* **1994**, *116*, 11931−11937.

(30) Choi, C.; Elber, R. Reaction path study of helix formation in tetrapeptides—effect of side chains. *J. Chem. Phys.* **1991**, *94*, 751−760.

(31) Fischer, S. Manuscript in preparation.

(32) Wilson, E. B., Jr.; Decius, J. C.; Cross, P. C. In *Molecular Vibrations*; Dover: New York, 1980.

(33) Atkins, P. W. In *Physical Chemistry*, 3rd ed.; Oxford University Press: Oxford, 1988.

(34) McQuarrie, D. A. In *Statistical Mechanics*; Harper Row: New York, 1976.

(35) Berne, B. J.; Borkovec, J. E.; Straub, J. E. Classical and modern methods in reaction rate theory. *J. Phys. Chem.* **1988**, *92*, 3711−3725.

(36) Hayward, J. A.; Reimers, J. R. Unit cells for simulation of hexagonal ice. *J. Chem. Phys.* **1997**, *106*, 1518−1529.

(37) Tidor, B.; Karplus, M. The contribution of vibrational entropy to molecular association: the dimerization of insulin. *J. Mol. Biol.* **1994**, *238*, 405−414.

(38) Baker, E. N.; Hubbard, R. E. Hydrogen bonding in globular proteins. *Prog. Biophys. Mol. Biol.* **1984**, *44*, 97−179.

(39) Hooft, R. W. W.; Sander, C.; Vriend, G. Positioning hydrogen atoms by optimizing hydrogen-bond networks in protein structures. *Proteins: Struct., Funct., Genet.* **1996**, *26*, 363−376.

(40) Sciortino, F.; Geiger, A.; Stanley, H. E. Effects of defects on molecular mobility in liquid water. *Nature* **1991**, *354*, 218−221.

(41) Agmon, N. Tetrahedral displacement—the molecular mechanism behind the debye relaxation in water. *J. Phys. Chem.* **1996**, *100*, 1072−1080.

(42) Smith, P. E.; vanSchaik, R. C.; Szyperski, T.; Wuthrich, K.; vanGunsteren, W. F. Internal mobility of the basic pancreatic trypsin inhibitor in solution—a comparison of NMR spin relaxation measurements and molecular dynamics simulations. *J. Mol. Biol.* **1995**, *246*, 356−365.

(43) Karplus, M.; Kushik, J. N. Method for estimating the configurational entropy of macromolecules. *Macromolecules* **1981**, *14*, 325−332.

(44) Chandler, D. Statistical mechanics of isomerization dynamics in liquids and the transition state approximation. *J. Chem. Phys.* **1978**, *68*, 2959.

(45) Fischer, S. Ph.D. Thesis, Harvard University, Cambridge, MA, 1992.

(46) Fischer, S.; Michnick, S.; Karplus, M. A Mechanism for rotamase catalysis by the FK506 binding protein (FKBP). *Biochemistry* **1993**, *32*, 13830−13837.

(47) Fischer, S.; Grootenhuis, P. D. J.; Groenen, L. C.; van Hoorn, W. P.; van Veggel, F. C. J. M.; Reinhoudt, D. N.; Karplus, M. Pathways for conformational interconversion of Calix[4]arenes. *J. Am. Chem. Soc.* **1995**, *117*, 1611−1620.

(48) Verma, C. S.; Fischer, S.; Hubbard, R. E. Manuscript in preparation.

(49) Denisov, V. P.; Venu, K.; Peters, J.; Horlein, H. D.; Halle, B. Orientational disorder and entropy of water in protein cavities. *J. Phys. Chem. B* **1997**, *101*, 9380−9389.